Int. J. Electrochem. Sci., 17 **(2022)** Article Number: 220312, doi: 10.20964/2022.03.44

International Journal of
ELECTROCHEMICAL
SCIENCE
www.electrochemsci.org

Short Communication

Corrosion Behavior of Mg-1.5Mn-2.0Y Alloy in Different Solutions

Li Liu[*], *Zhongxun Wang*, *Xiaofeng Gong*, *Zhihui Zang*, *Yanhui Wang*

Department of Mechanical Engineering, Yantai Vocational College, Yantai 264670, China
[*]E-mail: peonylotus2020@outlook.com

Received: 6 November 2021 / *Accepted:* 28 December 2021 / *Published:* 2 February 2022

Extruded Mg-1.5Mn-2.0Y alloy was prepared in this work. Microstructure and compositions of the alloy were analyzed through optical microscope and X-ray diffraction. Corrosion performance and morphology of the alloy in different solutions were evaluated. Mg-1.5Mn-2.0Y alloy consisted of α-Mg phase, α-Mn phase and $Mg_{24}Y_5$ phase. The corrosive properties of the solutions from strong to weak in proper order were: simulated body fluid, 3.5wt.% NaCl solution and 0.9wt.% NaCl solution. In the two NaCl solutions, the alloy exhibited the characters of pitting corrosion and filiform corrosion. In simulated body fluid, the alloy was covered with scaly corrosion products. In these two NaCl solutions, the electrochemical impedance spectroscopy was a capacitive arc. In simulated body fluid, an inductive arc was seen besides a capacitive arc. With increasing immersion time, the diameter of the impedance spectrum in simulated body fluid and 0.9wt.% NaCl solution gradually increased. The diameter of the impedance spectrum in 3.5wt.% NaCl solution increased at first and then decreased. A clear plateau was seen in each polarization curve. In 0.9wt.% NaCl solution, the alloy showed the largest breakdown potential.

Keywords: alloy; corrosion morphology; impedance spectroscopy; polarization

1. INTRODUCTION

The anticorrosion ability of pure Mg is so poor that it cannot be directly used as structural material [1, 2]. Mg alloy can be prepared by adding other elements to pure Mg. The Mg alloy is the lightest constructional material, which can be applied in areas like transportation and aircraft [3]. According to research findings, adding a proper amount Mn to pure Mg is good for to improve the anticorrosion ability of Mg [4]. Feng et al. studied the effect of solid solution treatment on the corrosion rate of Mg-xwt.% Mn (x=1.0, 2.0, 3.0) alloy in Hank's solution [5]. The results showed that, the optimum solid solution treatment temperature of the alloy rised with the increase in adding amount of Mn, and the proper solid solution treatment process improved anticorrosion ability. Adding rare earth element to Mg

can improve its mechanical property, anticorrosion ability and antioxygenic property [6]. Zhang et al. found that adding Ce enhanced the anticorrosion ability of AZ31 alloy [7]. Mg alloy with excellent anticorrosion ability can be produced by adding Mn and rare earth element to pure Mg.

In this work, Mg-1.5Mn-2.0Y alloy was obtained by adding Mn and Y to Mg. The corrosion performance of the alloy in 0.9wt.% NaCl solution, 3.5wt.% NaCl solution and simulated body fluid (SBF) were studied. The corrosion mechanism was discussed.

2. EXPERIMENTAL AND METHOD

Extruded Mg-1.5Mn-2.0Y alloy was used in this work. Mg, Mg-10wt.% Mn master alloy and Mg-21.5wt.% Y master alloy were used as raw materials. The steel crucible with the raw materials was put in the resistance furnace preheated to 720℃. Stirred the mixture until melted. The furnace was hold at 720℃ for a certain time. During heating, the furnace was filled with inert gas. The melt was poured into the mould. After the solidification process, Mg-1.5Mn-2.0Y alloy ingot was obtained. Then the ingot was extruded into bar with a diameter of 20 mm. Specimens was cut from the extruded rod.

Morphology and composition of the extruded Mg-1.5Mn-2.0Y alloy were revealed through microscope and X-ray equipment. Corrosion performance of the alloy in different corrosive media was analyzed. The corrosive media were 0.9wt.% NaCl solution, 3.5wt.% NaCl solution and SBF. Corrosion products were analyzed by X-ray. Morphology of the alloy was observed via scanning electron microscope after being corroded for seven days. Electrochemical impedance spectroscopy (EIS) test was measured at open circuit potential with an amplitude of 2.5mV. The range of scanning frequency was 10^5-0.1Hz. The data were collected at 2, 4, 6, 8 and 12h of immersion. Subsequently, the polarization measurement was performed at a scanning speed of 1mV/s. The electrochemical parameter values were revealed by EC-Lab software.

3. RESULTS AND DISCUSSION

The morphology and phase composition of extruded Mg-1.5Mn-2.0Y alloy are shown in Fig.1. As demonstrated in Fig.1a, the alloy is composed of strip grains, deformed grains and small amounts of equiaxed grains with nonuniform sizes. Some black particles are unevenly distributed throughout the alloy. In the extruding process, big grains were crashed to small grains. As exhibited in Fig.1b, the phase components of the alloy are $Mg_{24}Y_5$ phase, α-Mn phase and α-Mg matrix. The solid solubility of Mn in α-Mg matrix is small and Mn can be separated out from the α-Mg matrix easily as particles [8, 9]. So, the black particles in the alloy are α-Mn phase from α-Mg matrix. In Mg-1.5Mn-2.0Y alloy, rare earth Y is present in the form of $Mg_{24}Y_5$ phase.

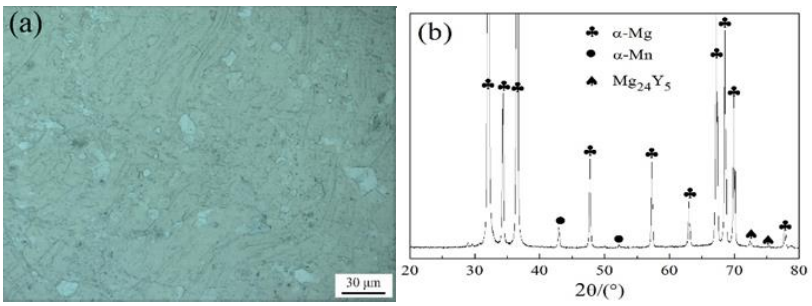

Figure 1. Morphology (a) and phase composition (b) of extruded Mg-1.5Mn-2.0Y alloy

The corrosion morphology of extruded Mg-1.5Mn-2.0Y alloy in different corrosive media are shown in Fig. 2. During corrosion, bubbles appeared the alloy surface. This demonstrates that hydrogen evolutional corrosion took place on alloy surface. As exhibited in Fig.2a and Fig.2b, in two NaCl solutions, the alloy has a characteristic of localized corrosion. Continuous layer of corrosion products is not seen on alloy surface. In 0.9wt.% NaCl solution, the alloy surface is humpy and hillocky, which shows obvious features of pitting corrosion and filiform corrosion. Several tiny holes are found in the part of the alloy surface without filiform corrosion. Cl^- has characters of small size and strong penetration. This causes pitting corrosion taking place in alloy surface [10]. The Cl^- adsorbed at the defects of the alloy causes pitting corrosion. Pitting corrosion leads to those different areas of the alloy surface have different corrosion rates [11]. After being corroded for seven days, different regions of Mg-1.5Mn-2.0Y alloy exhibits different degrees of corrosion. When immersed into aqueous solutions, oxidation film is formed on the alloy surface, thus forming micro-battery [12]. Therefore, filiform corrosion can also take place in the alloy surface. The microstructure of Mg-1.5Mn-2.0Y alloy is inhomogeneous, and the second phase $Mg_{24}Y_5$ is unevenly distributed in the alloy. As a result, the electrochemistry of the alloy surface is inhomogeneous. This inhomogeneous electrochemistry makes pitting corrosion expand to long strips of filiform corrosion. The corrosion level of Mg-1.5Mn-2.0Y alloy in 3.5wt.% NaCl solution is more severe than that in 0.9wt.% NaCl solution. After being corroded by 3.5wt.% NaCl solution, corrosion holes with larger diameters are seen in the alloy surface, and the area of alloy surface without filiform corrosion is smaller. It is concluded that increasing Cl^- concentration aggravates corrosion and not changes the type of corrosion.

The corrosion morphology of the alloy in SBF is much different from that in NaCl solution. In SBF (Fig.2c), total corrosion takes place in the alloy surface. The corrosion products appear as net type and scaly veil. The corrosion products layer with cracks is thick. The corrosivity of SBF is much stronger compared to the other two NaCl solutions. SBF seeps through corrosion products along cracks and goes on to corrupt the alloy.

From Fig.2, it is obtained that the corrosion rates of Mg-1.5Mn-2.0Y alloy in different solutions arrange from high to low as: SBF, 3.5wt.% NaCl solution and 0.9wt.% NaCl solution.

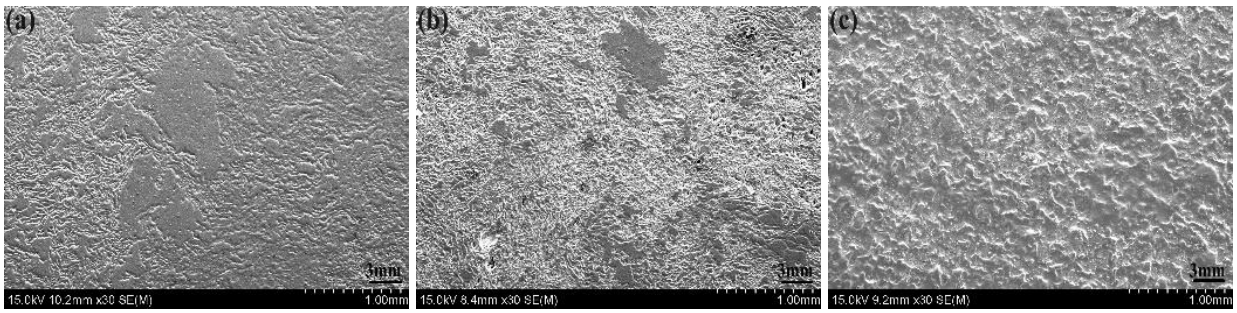

Figure 2. Morphology of Mg-1.5Mn-2.0Y alloy after being corroded for seven days in three solutions (a) 0.9wt.% NaCl, (b) 3.5wt.% NaCl, (c) SBF

The compositions of the corrosion products on Mg-1.5Mn-2.0Y alloy in different solutions are shown in Fig.3. After corrosion, $Mg(OH)_2$ phase was detected on the alloy surface. During immersion, the corrosion of α-Mg phase mainly took place on the alloy surface [13]. The corrosion reactions are as follows.

The hydrogen evolution reaction happened in the cathode.

$$2H_2O+2e^-\rightarrow H_2+2OH^- \quad (1)$$

The anodic reaction was the dissolution of α-Mg.

$$Mg-2e^-\rightarrow Mg^{2+} \quad (2)$$

The generation of corrosion products was due to the following reaction.

$$Mg^{2+}+2OH^-\rightarrow Mg(OH)_2 \quad (3)$$

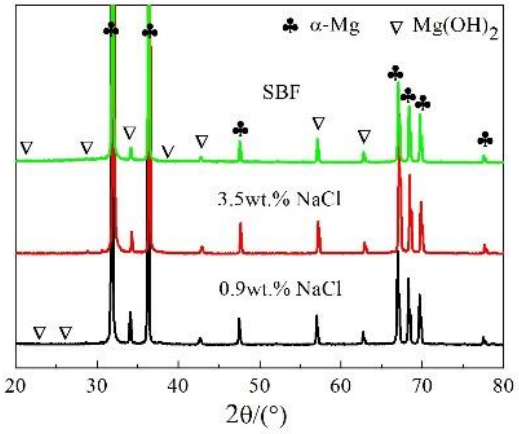

Figure 3. Compositions of corrosion products on Mg-1.5Mn-2.0Y alloy in different solutions

The EIS data collected at 2-12h are shown in Fig.4. In 0.9wt.% NaCl solution (Fig.4a), each EIS curve is a single capacitive arc, and the diameter of the capacitive arc increases with increasing immersion time. These mean the corrosion rate of the alloy changes with varying immersion time, but the corrosion mechanism doesn't change. In 3.5wt.% NaCl solution and 0.9wt.% NaCl solution, all EIS curves are similar in shape. This means increasing Cl^- concentration doesn't change the corrosion

mechanism. The larger the diameter of the capacitive arc, the lower the corrosion rate [14]. In 0.9wt.% NaCl solution, the corrosion rate of the alloy gradually reduces with increasing time. In immersion period, $Mg(OH)_2$ was deposited on alloy surface, which prevented NaCl solution from contact with alloy. As a result, the corrosion rate of the alloy was reduced. During immersion process, the prevention ability of the deposition layer increases with increasing time.

In 3.5wt.% NaCl solution, the diameter of the capacitive arc increases first and then decreases with increasing time. When immersion time is 2h, the capacitive arc shows the minimum diameter, and the alloy exhibits the largest corrosion rate. When immersion time is 4h, the capacitive arc shows the largest diameter, and the alloy exhibits the lowest corrosion rate. The corrosion rate of the alloy decreases and then increases with increasing time. Within 4h of immersion, corrosion product $Mg(OH)_2$ were continuously deposited on alloy surface. The $Mg(OH)_2$ layer acted as a barrier, keeping the alloy from touching the NaCl solution. As time increased, the $Mg(OH)_2$ layer became loose and caducous.

The equivalent electric circuit for EIS curves in NaCl solution is shown in Fig.5a. The relevant parameter values are listed in Table 1. R_s is solution resistance [15, 16]. CPE is the electric double-layer capacitor between alloy and NaCl solution. R_{ct} is charge transfer resistance. R_{ct} is in direct proportion to the diameter of capacitive arc [17]. Namely, the bigger the diameter of capacitive arc, the less resistance there is in charge transferring and the less the corrosion rate. In 0.9wt.%NaCl solution, the R_{ct} grows from 1265.4Ω·cm^2 at 2h to 2890.2Ω·cm^2 at 12h of immersion. The R_{ct} in 3.5wt.%NaCl solution is smaller than that in 0.9wt.%NaCl on the same immersion time. The corrosion rate of Mg-1.5Mn-2.0Y alloy in 0.9wt.%NaCl solution is lower than in 3.5wt.%NaCl solution.

As shown in Fig.4c, the shape of the EIS in SBF is very different from that in NaCl solution. This shows the corrosion mechanisms in SBF and NaCl solution are different. The result is consistent with analyses by Fig.2. In SBF for 2-12h, each EIS curve consists of a capacitive arc in high frequency and an inductance arc in low frequency. Its equivalent circuit is shown in Fig.5b. L is inductor, and R_L is the resistance of inductor [18]. The existence of inductance arc means that, during electrochemical process, the corrosion product layer on alloy surface shows bad compactness and it is broken [19]. The inductive characteristic in the EIS curve at 2h is not obvious. The inductive characteristic is obvious gradually with increasing time. This shows that, the longer the immersion time, the more the corrosion product layer on alloy surface. The R_{ct} in SBF is smaller than that in the two NaCl solutions, meaning the corrosion rate of Mg-1.5Mn-2.0Y alloy in SBF is larger than that in NaCl solutions.

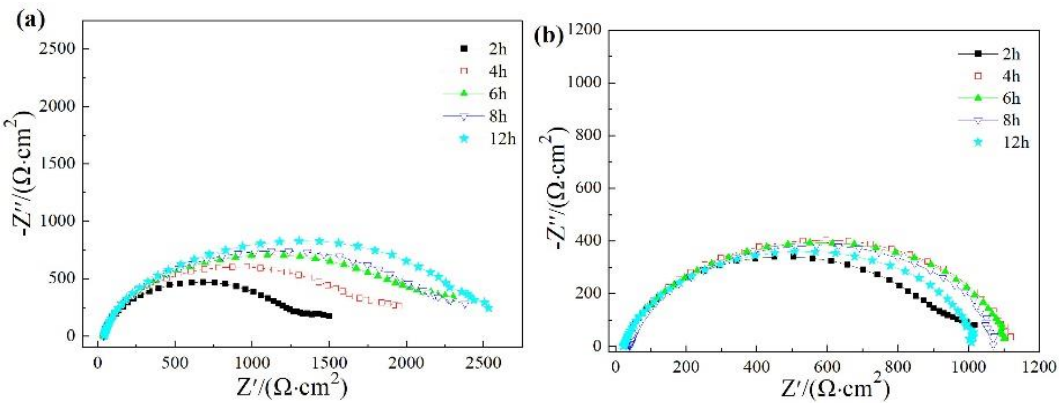

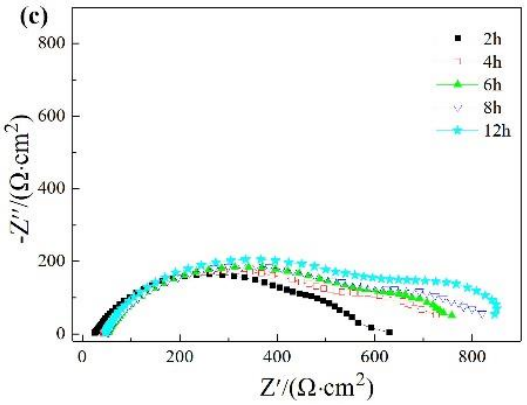

Figure 4. EIS data collected at 2-12h in different solutions(a) 0.9wt.% NaCl, (b) 3.5wt.% NaCl, (c) SBF

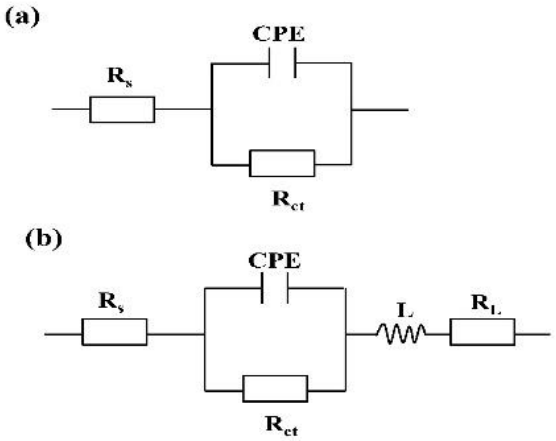

Figure 5. Equivalent circuit modes for EIS data in different solutions

Table 1. EIS parameters collected at 2-12h in different solutions

0.9wt.% NaCl	2h	4h	6h	8h	12h
R_s (Ω·cm^2)	35.1	35.6	36.9	39.5	42.7
R_{ct} (Ω·cm^2)	1265.4	1720.8	2715.5	2645.3	2890.2
3.5wt.% NaCl					
R_s (Ω·cm^2)	24.4	29.8	33.6	39.2	21.7
R_{ct} (Ω·cm^2)	976.9	1142.1	1117.7	1093.1	1013.8
SBF					
R_s (Ω·cm^2)	25.2	42.8	51.1	52.6	46.4
R_{ct} (Ω·cm^2)	489.8	645.8	716.7	769.4	794.6
R_L (Ω·cm^2)	89.4	103.1	75.7	98.7	50.5

The polarization curves of the alloy in different solutions are shown in Fig.6. The corrosion potential, corrosion current density, breakdown potential and anode Tafel slope are listed in Table 2.

The corrosion potentials in different solutions arrange from high to low as: 0.9wt.% NaCl solution, 3.5wt.% NaCl solution and SBF. The changing tendency of corrosion current density and corrosion potential is the quite opposite. The corrosion rate of the alloy in 0.9wt.% NaCl solution is smaller than that in other two solutions. In SBF, the alloy shows the largest corrosion rate. The result revealed by polarization is consistent with the analyses from corrosion morphology and EIS.

An obvious plateau can be seen in each anodic branch of polarization curve, which shows a protective corrosion product layer is formed on alloy surface during polarization. The plateau is limited by the breakdown potential related to the rupture of the protective corrosion product layer. In 0.9wt.% NaCl solution, the polarization curve has the widest plateau. This shows the corrosion product layer has the strongest protection ability. The breakdown potentials in 0.9wt.% NaCl solution, 3.5wt.% NaCl solution and SBF are -340mV, -916mV and -1452mV, respectively. The corrosion product layer in SBF is the least stable and the easiest to lose protection ability. The penetrability of Cl^- with small radius is so strong that pitting corrosion took place on corrosion product layer. Reaction is as follows [20].

$$Mg(OH)_2+2Cl^-\rightarrow MgCl_2+2OH^- \quad (4)$$

Hydroxyapatite ($Ca_{10}(PO_4)_6(OH)_2$) can be spontaneously precipitated from SBF. The solubility of $Ca_{10}(PO_4)_6(OH)_2$ in the solution with high pH is low [21]. When Mg-1.5Mn-2.0Y was immersed into SBF, the pH of the solution near the alloy increases with the corrosion of α-Mg. $Ca_{10}(PO_4)_6(OH)_2$ is formed by the following reaction.

$$10Ca^{2+}+6PO^{4-}+2OH^-\rightarrow Ca_{10}(PO_4)_6(OH)_2 \quad (5)$$

The reaction (5) consumes a certain amount of OH^-, which promotes the reaction (4). So in SBF, the corrosion product layer is easy to be damaged.

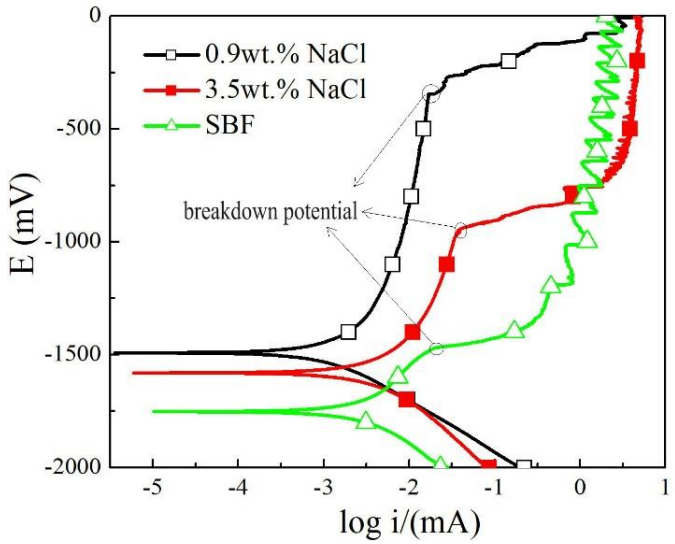

Figure 6. Polarization curves of Mg-1.5Mn-2.0Y alloy in different solutions

Table 2. Corrosion potential, corrosion current density, breakdown potential and anode Tafel slope in different solutions

solution	corrosion potential (mV)	corrosion current density (mA/cm^2)	breakdown potential (mV)	anode Tafel slope (mV/dec)
0.9wt.% NaCl	-1492	2.5×10^{-3}	-340	99
3.5wt.% NaCl	-1579	8.1×10^{-3}	-916	137
SBF	-1752	12.8×10^{-3}	-1452	157

4. CONCLUSIONS

Extruded Mg-1.5Mn-2.0Y alloy was applied in this work. The corrosion behavior of this alloy in 0.9wt.% NaCl solution, 3.5wt.% NaCl solution and SBF was investigated. The main conclusions are as follows.

(1) The corrosion rates of the alloy in different solutions arranged from high to low as: SBF, 3.5wt.% NaCl solution and 0.9wt.% NaCl solution.

(2) In 0.9wt.% NaCl solution and 3.5wt.% NaCl, the corrosion types of the alloy were similar. Pitting corrosion and filiform corrosion took place in the alloy surface. In SBF, total corrosion took place in the alloy surface.

(3) An obvious passivation zone could be seen in each polarization curve. In 0.9wt.% NaCl solution, the alloy had the highest corrosion potential, smallest corrosion current density and highest breakdown potential.

ACKNOWLEDGEMENTS
This work was supported by the Doctoral Fund of Yantai Vocational College (2020001), School-based Research of Yantai Vocational College (2020XBZD002) and the Project of Shandong Province Higher Educational Science and Technology Program (J17KB039).

References

1. M. P. Gomes, I. Costa, N. Pébère, L. R. Jesualdo, T. Bernard and V. Vincent, *Electrochim Acta*, 306 (2019) 61.
2. A. Atrens, Z. Shi, S. Umehreen, S. Johnston, G. L. Song, X. Chen and F. Pan, *J Magnes Alloy*, 8 (2020) 989.
3. Z. Y. Ding, L. Y. Cui, R. C. Zeng, Y. B. Zhao, S. K. Guan, D. K. Xu and C.G. Lin, *J Mater Sci Technol.,* 34 (2018) 1550.
4. D. D. Gu, J. Peng, J. W. Wang, Z. T. Liu and F. S. Pan, *Acta Metall Sin.*, 34 (2021) 1.
5. Z. Feng, L. P. Yan, H. Ding, T. S. Yang and D. M. Zhai, *Light Alloy Fabrica Technol.*, 45 (2017) 55.
6. H. Azzeddine, A. Hanna, A. Dakhouche, L. Rabahi and T. Baudin, *J Alloy Compd.*, 829 (2020) 154569.
7. C. Zhang, L. Wu, G. Huang, K. Liu and F. Pan, *J Electrochem Soc.*, 166 (2019) C445.

8. C. Zhou, Y. Liu, H. Zhang, X. Chen and Y. Li, *Metall Mater Trans* A, 51 (2020) 3238.
9. A. Bahmani, S. Arthanari and K. S. Shin, *J Magnes Alloy*, 7 (2019) 38.
10. N. Palaniappan, I. S. Cole and A. E. Kuznetsov, *Rsc Adv.*, 10 (2020) 11426.
11. L. Liu, Y. Y. Jia, J. T. Jiang, B. Zhang and L, *J Alloy Compd.*, 799 (2019) 1.
12. Z. Y. Ding, L. Y. Cui, R. C. Zeng, Y. B. Zhao, S. K. Guan, D.K. Xu and C.G. Lin, *J Mater Sci Technol.,* 34 (2018) 1550.
13. S. V. Lamaka, B. Vaghefinazari, M. Di, R. P. Petrauskas and M. L, Zheludkevich, *Corros Sci.*, 128 (2017) 224.
14. J. Yang, C. Blawert, S. V. Lamaka, K. A. Yasakau and M. L. Zheludkevich, *Corros Sci.*, 142 (2018) 222.
15. S. A. Abdel-Gawad and M. A. Shoeib. *Surf Interfaces*, 14 (2019) 108.
16. W. Jiang, J. Wang, W. Zhao, Q. Liu, D. Jiang and S. Guo, *J Magnes Alloy*, 7 (2019) 15.
17. P. P. Wu, F. J. Xu, K. K. Deng, F. Y. Han, Z. Z. Zhang and R. Gao, *Corros Sci.*, 127 (2017) 280.
18. S. Yin, W. Duan, W. Liu, L. Wu and Z. Zhang, *Corros Sci.*, 166 (2019) 108419.
19. C. Q. Li, D. K. Xu, X. B. Chen, B. J. Wang, R. Z. Wu, E. H. Han and N. Birbilis, *Electrochim Acta*, 260 (2018) 55.
20. Q. Zhang, Q. Li and X. Chen, *Rsc Adv.*, 10 (2020) 43371.
21. D. Mei, S. V. Lamaka, J. Gonzalez, F. Feyerabend, R. Willumeit-Römer and M. L. Zheludkevich, *Corros Sci*., 147 (2019) 81.